

Article

A Comparison Study on Wear Behaviors of Mo and Al₂O₃-Mo Coatings from RT to 300 °C

Jianhui Yan ^{1,2}, Yuanjun Guo ^{1,2,*}, Yi Wang ^{1,2}, Peng Zhou ^{1,2} and Jingwen Qiu ^{1,2}

¹ School of Material Science and Engineering, Hunan University of Science and Technology, Xiangtan 411201, China; yanjainhui88@163.com (J.Y.); ywang312@hnust.edu.cn (Y.W.); zhoupeng1987825@sina.com (P.Z.); qjwesu@foxmail.com (J.Q.)

² Hunan Provincial Key Defense Laboratory of High Temperature Wear Resisting Materials and Preparation Technology, Hunan University of Science and Technology, Xiangtan 411201, China

* Correspondence: yjguo@hnust.edu.cn

Received: 11 April 2018; Accepted: 8 May 2018; Published: 11 May 2018



Abstract: Mo and Al₂O₃-Mo coatings are fabricated on a low-carbon steel substrate using atmospheric plasma spraying. The microstructure and mechanical properties of two as-sprayed coatings, with a particular focus on the tribological behaviors from room temperature to 300 °C, are comparatively investigated in this study. Microstructural analysis of the coatings shows that the porosity of the Al₂O₃-Mo coating is higher than that of Mo coating. The addition of Al₂O₃ particles reduces the coating–substrate adhesion strength. The Al₂O₃-Mo coating, in comparison to the Mo coating, shows improved mechanical properties, such as hardness and wear resistance. The friction coefficients of both coatings increase with further increases in test temperatures. The friction coefficient of the Al₂O₃-Mo coating, tested above 100 °C, is lower than that of the Mo coating. The wear failure mechanisms of the two coatings are delamination, brittle fracture, oxidation and adhesion wear. In addition, local plastic deformation was also found in the Mo coating.

Keywords: atmospheric plasma spraying; molybdenum coating; Al₂O₃; wear resistance

1. Introduction

Molybdenum (Mo) coatings are used to improve underlying materials' mechanical properties and to decrease their wear. They show excellent scuffing resistance to abrasive wear, as well as high corrosion resistance [1–3]. The wear resistance of hardened steel coated with a Mo coating could be enhanced by a factor of 2–18 [4]. Because of the excellent tribological properties, Mo coatings are widely used in automobile, aerospace, and pulp and paper industries to protect machine parts from wear and corrosion [5,6].

Thermal spraying is an advantageous deposition process that deposits a Mo layer on various substrate materials. Flame spraying is usually used to fabricate Mo coatings. However, it has a short service lifetime and low cohesive strength [7]. Plasma-sprayed Mo coatings have a low hardness of 300 HV, which results in very poor wear resistance [8]. To address these shortcomings, MoSi₂, brass, Mo₂C, NiCrBSi, and TiN were introduced into plasma-sprayed Mo coatings to improve wear resistance [5,9–11]. However, the wear resistance of these Mo matrix composite coatings is also very limited. In other words, new Mo matrix composite coatings, which motivate the current work, should be developed.

The atmospheric plasma spraying (APS) technique endows an Al₂O₃ coating with high hardness, outstanding corrosion and good wear resistance, and excellent chemical stability under critical application conditions [12]. Therefore, a plasma-sprayed Al₂O₃ coating on metallic substrates has been widely used as a wear-resistant coating in engineering fields [13,14]. The close coefficient of thermal

expansion (CTE) between Mo ($6.7 \times 10^{-6}/\text{K}$) and Al_2O_3 ($6.8 \times 10^{-6}/\text{K}$) could reduce the thermal stress between the two phases boundaries. This leads to fewer micro cracks in the material. Meanwhile, it was reported that $\text{Al}_2\text{O}_3/\text{Mo}$ composites, fabricated using powder metallurgy, have excellent toughness and wear resistance [15]. The above-mentioned studies suggested that the $\text{Al}_2\text{O}_3\text{-Mo}$ coating could be a good alternative candidate in providing excellent wear resistance.

To reach a more efficient performance, modern engine pistons usually operate under higher temperatures. The temperature of the environment is an important factor in evaluating the tribological characteristics of a piston ring-coating material. However, in previous literature there is almost no research on the wear of plasma-sprayed Mo coatings integrated with Al_2O_3 particles, especially at room temperature (RT) to 300 °C. In the present research, Mo coatings, with and without reinforced Al_2O_3 dopant, were fabricated using APS, in an attempt to assess the microstructure, mechanical properties and wear behaviors (RT to 300 °C) of the two coatings.

2. Materials and Experimental Procedure

2.1. Feedstock Powders and Coatings Preparation

Commercial spray powders, i.e., Mo powder (38–75 μm) and Al_2O_3 powder (38–75 μm), were provided by Beijing Sunspraying Technology Co. Ltd. (Beijing, China). A monolithic Mo coating was fabricated with pure Mo powders. The mixed powders, for the spraying of the $\text{Al}_2\text{O}_3\text{-Mo}$ coating, consisted of 30 wt. % Al_2O_3 and 70 wt. % Mo powders. The composite powders were mechanically mixed for 20 h in order to obtain a uniform composite powder.

The Q235 Low-carbon steel (C: 0.16 wt. %; Mn: 0.45 wt. %; Si: 0.28 wt. %; S: 0.038 wt. %; P: 0.035 wt. %; tensile strength: 416 MPa; yield strength: 282 MPa; elongation: 29.6%; 130 HB) was used as a substrate. The Low-carbon steel substrates were previously grit-blasted using aluminum oxide (with a grit size of 36 mesh) under 0.65 MPa pressure, resulting in a surface roughness in the order of $R_a = 6 \mu\text{m}$. Mo and $\text{Al}_2\text{O}_3\text{-Mo}$ coatings on the low-carbon steel substrate were fabricated using APS technology. The APS equipment (APS-2000), plasma spray gun (PQ-1S), copper anode (nozzle), and tungsten cathode were provided by Beijing Aeronautical Manufacturing Technology Research Institute Manufacturer of China. An argon–hydrogen mixture was used as the plasma-forming gas. The spraying parameters for $\text{Al}_2\text{O}_3\text{-Mo}$ and Mo coatings are the same, and are listed in Table 1.

Table 1. Atmospheric plasma spraying parameters.

| Items | Parameters |
|------------------------|-------------|
| Ar flow rate | 45 L/min |
| H_2 flow rate | 6.5 L/min |
| Arc current | 500 A |
| Powder feeding rate | 60~65 g/min |
| Spraying distance | 110 mm |

2.2. Microstructures Characterization of Coatings

The phase compositions of the coatings were characterized via X-ray diffraction (XRD) with a $\text{Cu-K}\alpha$ radiation of 0.154 nm in wavelength at a scan speed of $2^\circ/\text{min}$ (D8 Discover 2500, Bruker Corporation, Karlsruhe, Germany). A scanning electron microscope (SEM, JSM-6380LV, JEOL Ltd., Tokyo, Japan) equipped with an energy dispersive spectroscope (EDS, JEOL Ltd., Tokyo, Japan) was used to analyze the microstructure, morphologies of the coatings, and the wear tracks. The porosities of the coatings were evaluated by image analysis of SEM images (at a magnification of $500\times$) of the cross-section of the polished samples [16]. For each cross-section, 15 images were measured for average measurement values.

2.3. Mechanical Properties Test

Micro-hardness measurements of the coatings were determined on the polished cross-sections using a Digital Micro-Vickers Hardness Tester (HVS-1000, Jinan Liangong Testing Technology Corporation of China, Jinan, China) under a normal load of 50 g and a dwell time of 15 s. Measurements were carried out for each sample at least 20 times to obtain an average value. The adhesion strengths of the coatings were measured using a direct pull-off tensile method according to ASTM C633, using an Instron 3369 electronic universal testing machine [17]. Before the tests, both sides of the coating samples were bonded to the low-carbon steel by using epoxy resin (E-7, provided by Shanghai Research Institute of Synthetic Resins, Shanghai, China). The adhesion strength of the epoxy resin in the C633 test configuration was about 65 MPa. The tensile load was applied at a constant loading rate of 1.0 mm/min until the sample was broken. Adhesion strength can be calculated by dividing the maximum force by the surface zone of the samples. The reported adhesion strength was the mean value of 5 samples sprayed with the same parameters.

2.4. Friction and Wear Test

Friction and wear tests were carried out in a ball-on-disk contact configuration tribometer (HSR-2M, Lanzhou, China) under dry conditions. The commercially available steel ball; with a diameter of 5 mm, $R_a = 0.8 \mu\text{m}$, and a hardness (HRC) of 48; was used as the upper specimen. The as-sprayed coating samples were used as the lower specimens. Prior to sliding tests, the as-sprayed coatings were mechanically ground using SiC emery papers to achieve the roughness (R_a) of $1.6 \mu\text{m}$. The coatings surface slides against the steel ball in a linear back-and-forth sliding motion. The sliding tests were conducted under a normal load of 30 N, a sliding time of 60 min, a stroke length of 5 mm, a speed of 50 mm/s, and a stroke frequency of 5 Hz. The test temperatures were RT, 100 °C, 200 °C, and 300 °C. The friction coefficients were dynamically recorded by an online automatic measurement. The wear depths and widths as well as the wear volume loss of the coatings were analyzed using a three-dimensional surface profiler (NanoMap-500LS, AEP Technology, Inc., Santa Clara, CA, USA). The wear rate is calculated as: $K = V/SF$, where K is the volume wear rate (mm^3/Nm), V is the wear volume (mm^3), S is the total sliding distance (m), and F is normal load (N).

3. Results and Discussion

3.1. Microstructure of As-Sprayed Coatings

Figure 1a,b shows SEM micrographs of the Mo powder and Al_2O_3 powder, respectively. It can be seen that the Mo powder is near-spherical in shape, showing a typical morphology of agglomerating and sintering particulates. The Al_2O_3 powders show an irregular morphology because they were processed by sintering and crushing. Both Mo and Al_2O_3 powders show good fluidity. The fluidity of the mixed powders was not changed in an obvious manner when Mo powders were mixed with 30 wt. % Al_2O_3 powders.

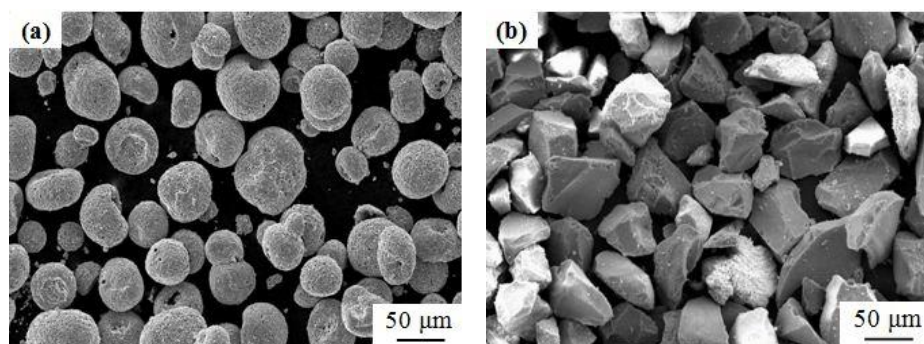


Figure 1. SEM morphologies of feedstock powders of (a) Mo powders and (b) Al_2O_3 powders.

XRD patterns of the raw powders, as-sprayed Mo, and Al₂O₃-Mo coatings, are shown in Figure 2. The Mo coating is composed of Mo and traces of MoO₃ phases, and the Al₂O₃-Mo coating mainly consisted of Mo, Al₂O₃ and traces of MoO₃ phases. The existence of MoO₃ phase in the two coatings was caused by the oxidation of Mo particles during the APS process [18]. Metal oxides usually reside along the splat boundaries of as-sprayed Mo coatings, and could enhance the hardness and tribological properties of coatings [19].

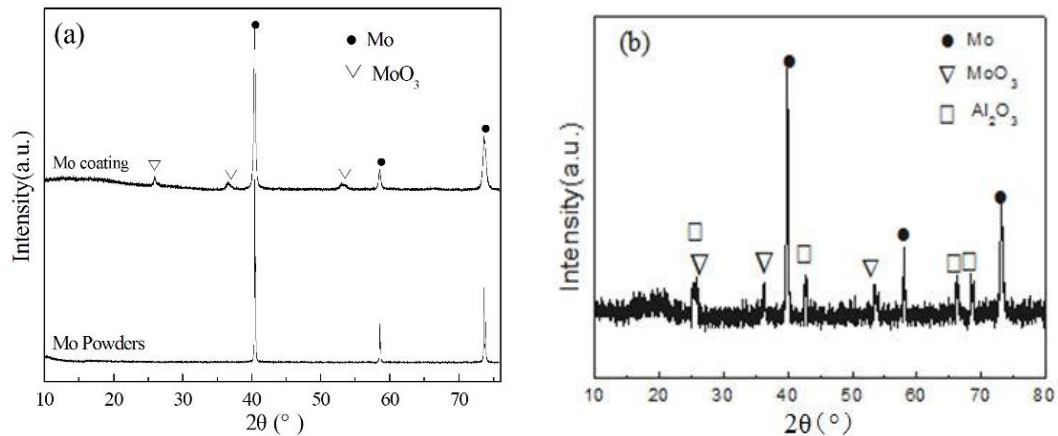


Figure 2. XRD patterns of coatings (a) Mo coating, and (b) Al₂O₃-Mo coating.

Figure 3 shows the surface and cross-section SEM morphologies of two kinds of coatings. As shown in Figure 3a,b, it is clear that the surfaces of both the Mo and Al₂O₃-Mo coatings consist of well-flattened splats, spherical features, insufficiently-flattened protuberances, and some pores, exhibiting the typical characteristics of plasma spray coatings. Some liquid droplets splashed when they were sprayed on the substrate surface. The splashed liquid particles subsequently changed to small spherical particles due to the effects of surface energy in the cool re-depositing process. Thus, the spherical particles were observed on the surface of the coatings. Figure 3c,d shows the cross-sectional morphologies of the Mo and Al₂O₃-Mo coatings, respectively. It is obvious that two coatings were stably bonded to the steel substrate without an interfacial decohesion, cracks, or pores. The typical splat and lamellar microstructure, some pores, and micro-cracks were also observed in the two as-sprayed coatings. The inherent characteristics of thermal sprayed technology inevitably result in the existence of microstructure defects in the coating [20]. The porosity proportion of the Mo and Al₂O₃-Mo coatings, estimated by the image analysis, are about (7.2 ± 0.3)% and (10.2 ± 0.5)%, respectively. This is attributed to the better spreadability of the melt Mo particles than the Al₂O₃ particles. The addition of Al₂O₃ particles increased the porosity of the as-sprayed Mo coating, which could influence the mechanical properties of the Mo coating, such as adhesion strengthen, hardness and wear resistance.

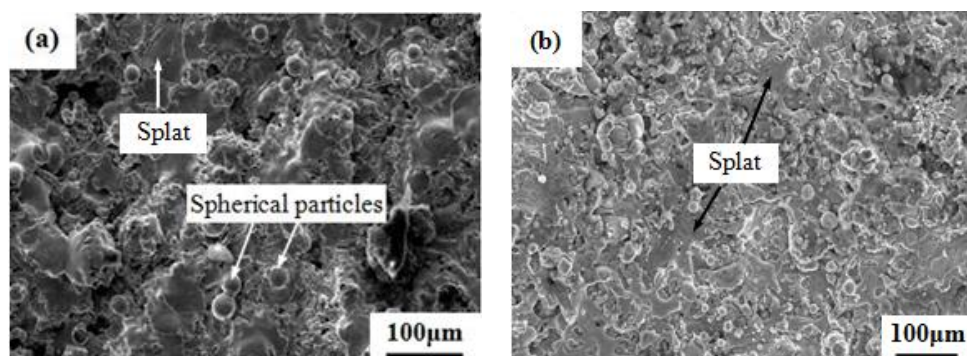


Figure 3. Cont.

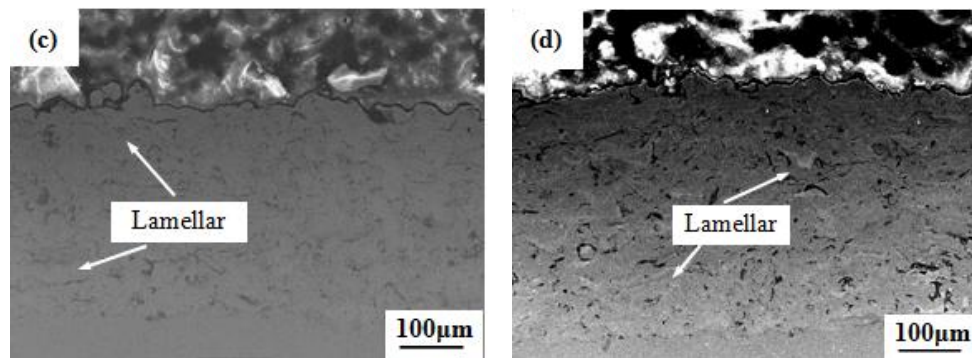


Figure 3. SEM microstructure of the as-sprayed coatings: (a) surface morphology of Mo; (b) surface morphology of Al₂O₃-Mo; (c) cross-sectional morphology of Mo; and (d) cross-sectional morphology of Al₂O₃-Mo.

3.2. Adhesion Strength and Micro Hardness of Coatings

The adhesion strengths of the coated specimens were measured, as shown in Figure 4. The adhesion strength of the as-sprayed Mo coating is about 43.8 ± 3.2 MPa, and that of Al₂O₃-Mo coating is approximately 33.6 ± 2.8 MPa. The average adhesion strength of pure Al₂O₃ coating, with substrate prepared by APS, is 26.9 ± 1.8 MPa [14]. It is obvious that Al₂O₃ decreased the adhesion strength of the as-sprayed Mo coating. After the adhesion strength test, the separated surfaces of the test samples revealed that the two kinds of coatings were not cohesively separated from the boundary of the splats but rather from the boundary between the coating and substrate. This shows that the adhesion strength among splats is better than that of the boundary between the coating and substrate. The metal Mo has a good bond performance with other materials [6]. When the Mo powders are used for spraying, the particles may be sufficiently melted and will strongly adhere to the rough surface of the substrate. For the Al₂O₃-Mo coating, the insufficiently-flattened Al₂O₃ particles had an adverse influence on the mechanical interlocking between splats or between the coating and substrate. Therefore, the addition of Al₂O₃ decreased the adhesion strength of Mo coating.

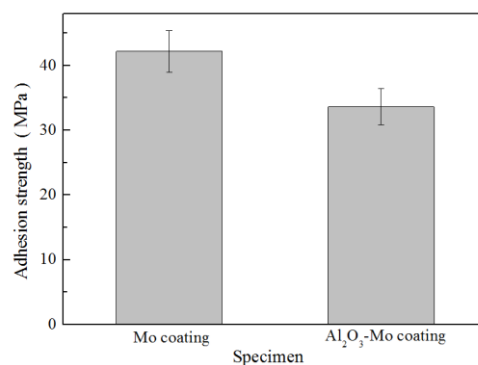


Figure 4. Adhesion strengths of the as-sprayed Mo and Al₂O₃-Mo coatings.

The micro-hardness values of both coatings, measured using a standard rectangular pyramid diamond indenter ($136 \pm 0.5^\circ$), are shown in Figure 5. The micro hardness of the Mo coating is about 3.12 ± 0.12 GPa (HV) and that of Al₂O₃-Mo coating is about 4.66 ± 0.16 GPa (HV). It is well known that Al₂O₃ ceramic is an attractive wear-resistant material because of its high hardness, and its elastic modulus (398.2 GPa [21]), which is much higher than that of Mo (310 GPa [22]). In general, the cracks, porosity, and poor adhesion between splats, decrease the micro hardness of the sprayed coatings [23]. However, as-sprayed pure Al₂O₃ coating has a hardness of about 13 GPa (HV) [14]. With the addition of 30 wt. % Al₂O₃ particles to the Mo coating, the micro-hardness of the as-sprayed Al₂O₃-Mo composite coating showed an increase of 49.5%, compared to that of the as-sprayed Mo coating.

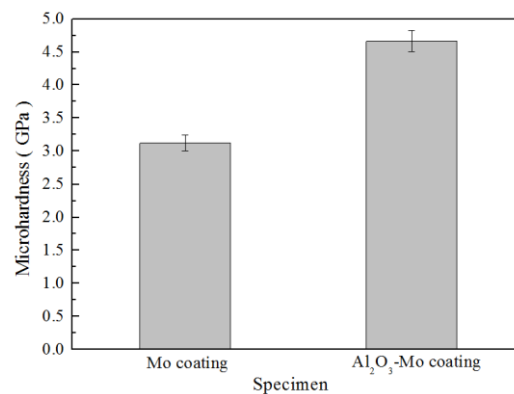


Figure 5. Micro hardness of the as-sprayed Mo and Al₂O₃-Mo coatings.

3.3. Friction Coefficient and Wear Rate of Coatings

The relation between the friction coefficient and time, and the average friction coefficients of both coatings at different test temperatures, are presented in Figure 6. It can be seen that the coefficients of friction–time curves of two coatings have similar trends. In other words, the friction coefficients are in a relative steady-state stage after a short running-in period. To reduce the measured deviation, the friction coefficient of each specimen was tested three times. As the wear test temperatures increased from RT to 300 °C, the average values of the friction coefficient for the Mo coating increased from 0.52 to 1.14, and that of the Al₂O₃-Mo coating increased from 0.75 to 1.05. Interestingly, compared to the Mo coating, the Al₂O₃-Mo coating showed higher average friction coefficients at RT. However, the Al₂O₃-Mo coating exhibits lower average friction coefficients at the other test temperatures, which indicated that the Al₂O₃ had a lubricating effect. The lubricating effect of the ceramics was also found in the as-sprayed ZrO₂-MoSi₂ coating, at a high temperature of 1100 °C [24].

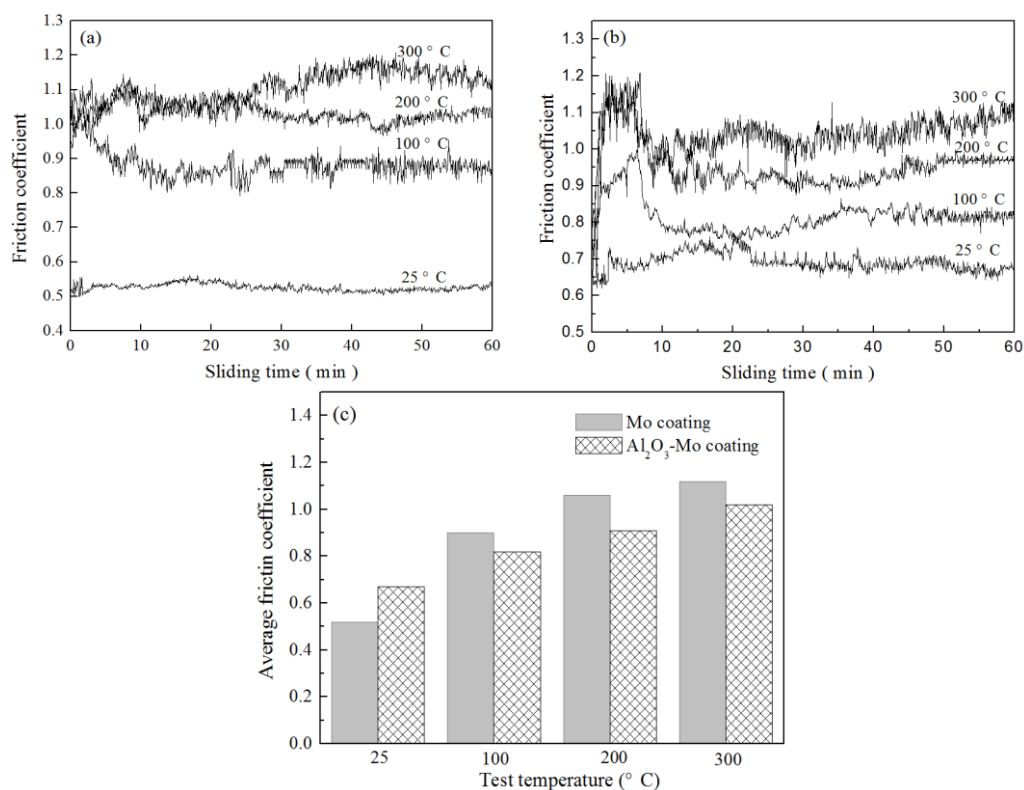


Figure 6. Friction coefficients tested at different temperatures of two coatings: (a) Mo; (b) Al₂O₃-Mo; (c) average friction coefficients.

Figure 7 shows the two-dimensional profiles of wear tracks for the Mo and Al₂O₃-Mo coatings at a test temperature of 300 °C. The measuring direction of the two-dimensional profile is vertical to the wear tracks. The wear profiles of the coated specimens for other test temperatures are not shown here for the sake of brevity. As shown in Figure 7, it can be seen that the width and depth of the scratches on the Mo coating are approximately 1750 μm and 110 μm, respectively. Whereas for the Al₂O₃-Mo coating, they are about 1250 μm and 56 μm, respectively. The profiles of these wear tracks show less wear volume for the Al₂O₃-reinforced Mo coating. The wear rates of both coatings at different test temperatures are shown in Figure 8. Their wear rate values at each test temperature are approximately 10⁻⁵ mm³/Nm. It can be seen that the wear rates of both coatings increase with the increase in test temperatures. As shown in Figure 8, the wear rate of the as-sprayed Mo-Al₂O₃ coating is less than that of the Mo coating when they were tested under the same conditions, especially in the test temperature of 100~300 °C. This indicates that the addition of 30 wt. % Al₂O₃ enhances the wear resistance of Mo coating from RT to 300 °C.

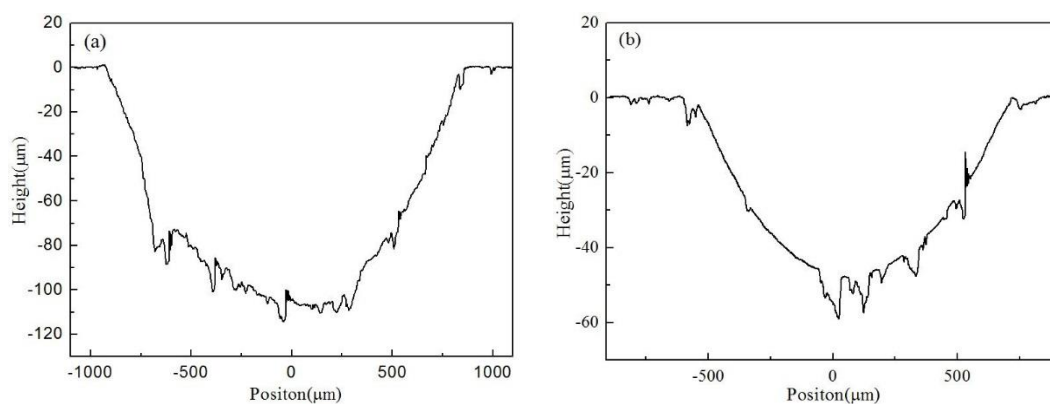


Figure 7. Two-dimensional wear scar morphologies at a test temperature of 300 °C: (a) Mo coating, and (b) Al₂O₃-Mo coating.

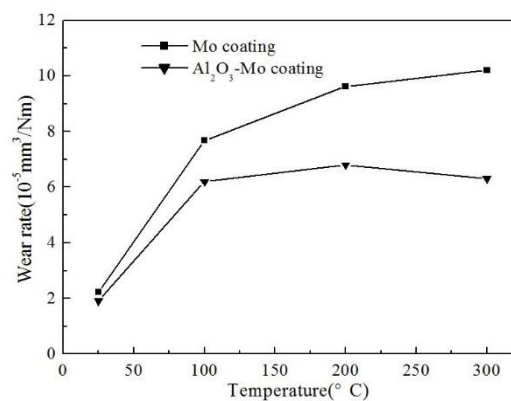


Figure 8. Wear rates of Mo and Al₂O₃-Mo coatings at different test temperatures.

3.4. Wear Mechanisms of Coatings

Figure 9 presents the SEM morphologies of the worn surface of the Mo coating after RT, 100 °C, 200 °C and 300 °C wear tests. A wear scar was commonly observed on the surface of plasma sprayed Mo coating, and the width and depth of the scar increased with the increase in test temperatures. As shown in Figure 9, splat delamination, brittle fracture and local plastic deformation were typically found in all specimens, regardless of wear test temperature. When a repeated load of 30 N was applied on the Mo coating surface, surface fatigue occurred in the coating. A crack easily initiated and gradually propagated below the surface, resulting in decohesion of the splat and delamination.

The abrasive wear mechanism, perhaps, occurs at the boundary between splats, where the adhesion strength is weaker than that within the splat, especially in the coating microstructure by thermal spraying [25,26]. In addition, a load applied to the steel counterpart caused an abrasive effect on the Mo coating. Therefore, plastic deformation zones also usually formed.

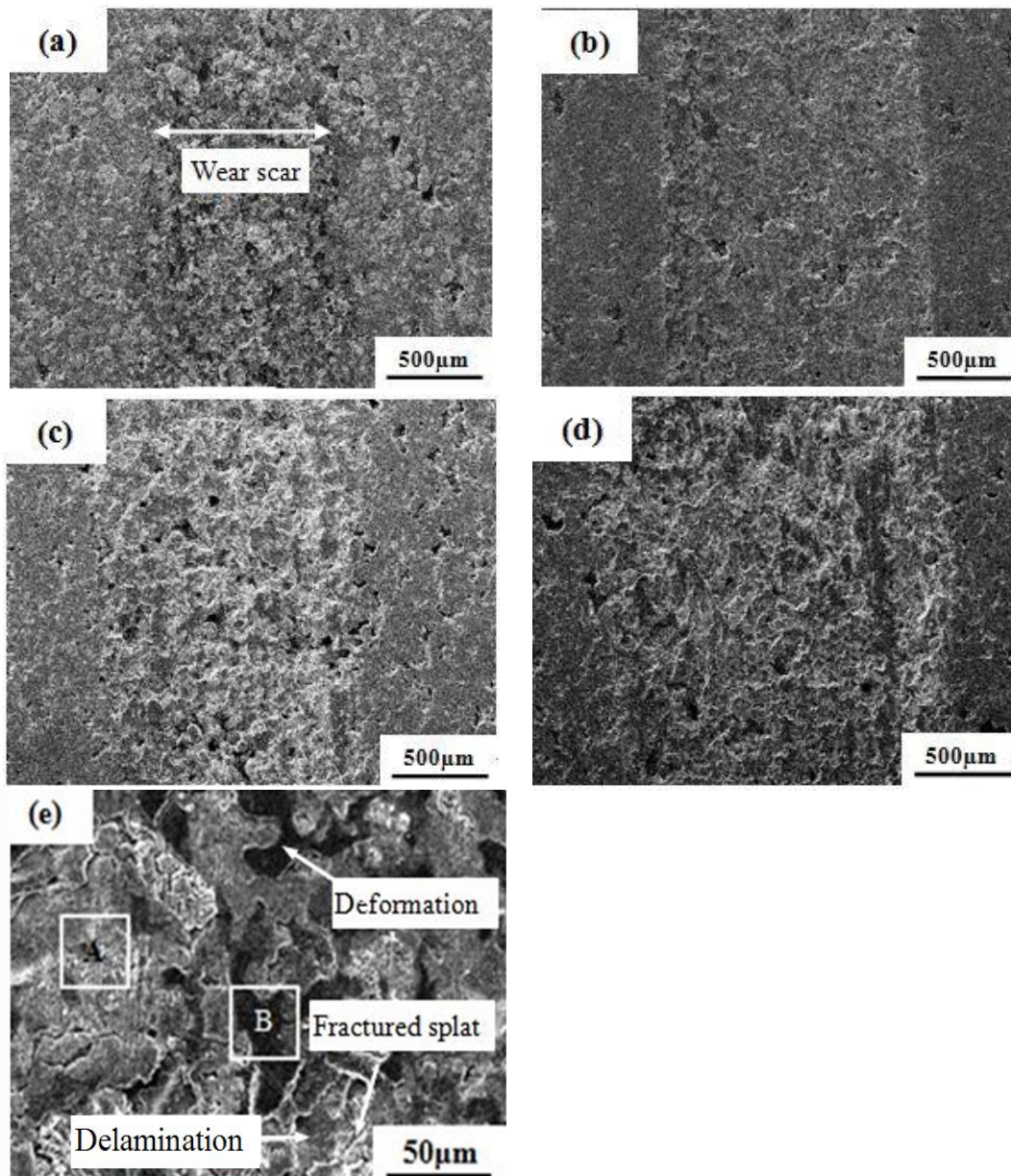


Figure 9. SEM morphologies of worn surface for Mo coating at different temperatures: (a) RT; (b) 100 °C; (c) 200 °C; (d) 300 °C; (e) high-magnification morphology of (d).

In addition, delamination and brittle fracture of Mo splats usually occurred in the Mo coating. Some pores and cracks existed in the as-sprayed coating. These crack-initiation regions usually endure discontinuous strain or compressive stress during wear tests. Once the stress exceeds the fatigue limit of the Mo coating, during the cyclic contact process, cracks will be nucleated and propagated. Once the cracks connected and coalesced with one another, the particles pulled-out, fatigue delamination took place in these sites, and the brittle fracture was finally developed [25]. The inner cracks within the Mo splat caused the embrittlement of Mo material, which occasionally generated brittle fracture damage.

Consequently, the contribution of Mo fracture resulted in degraded tribological property. Moreover, as displayed in Figure 9, splat delamination, brittle fracture and local plastic deformation occurred more and more frequently as wear test temperatures increased.

Figure 10 shows SEM micrographs of the worn surface of the Al_2O_3 -Mo coating after different temperature wear tests. As seen in Figure 10a–d, the wear scars widths increase with increases in the test temperature. In comparison to the Mo coating, the worn surface of the Al_2O_3 -Mo coating shows similar characteristics, such as delamination and brittle fracture. However, plastic deformation was hardly found on the worn surface. Under the same wear test conditions, the widths and depths of the wear scar for the Al_2O_3 -Mo coating were smaller than those observed on the worn surface of the Mo coating, indicating the Al_2O_3 -Mo coating had a superior wear resistance.

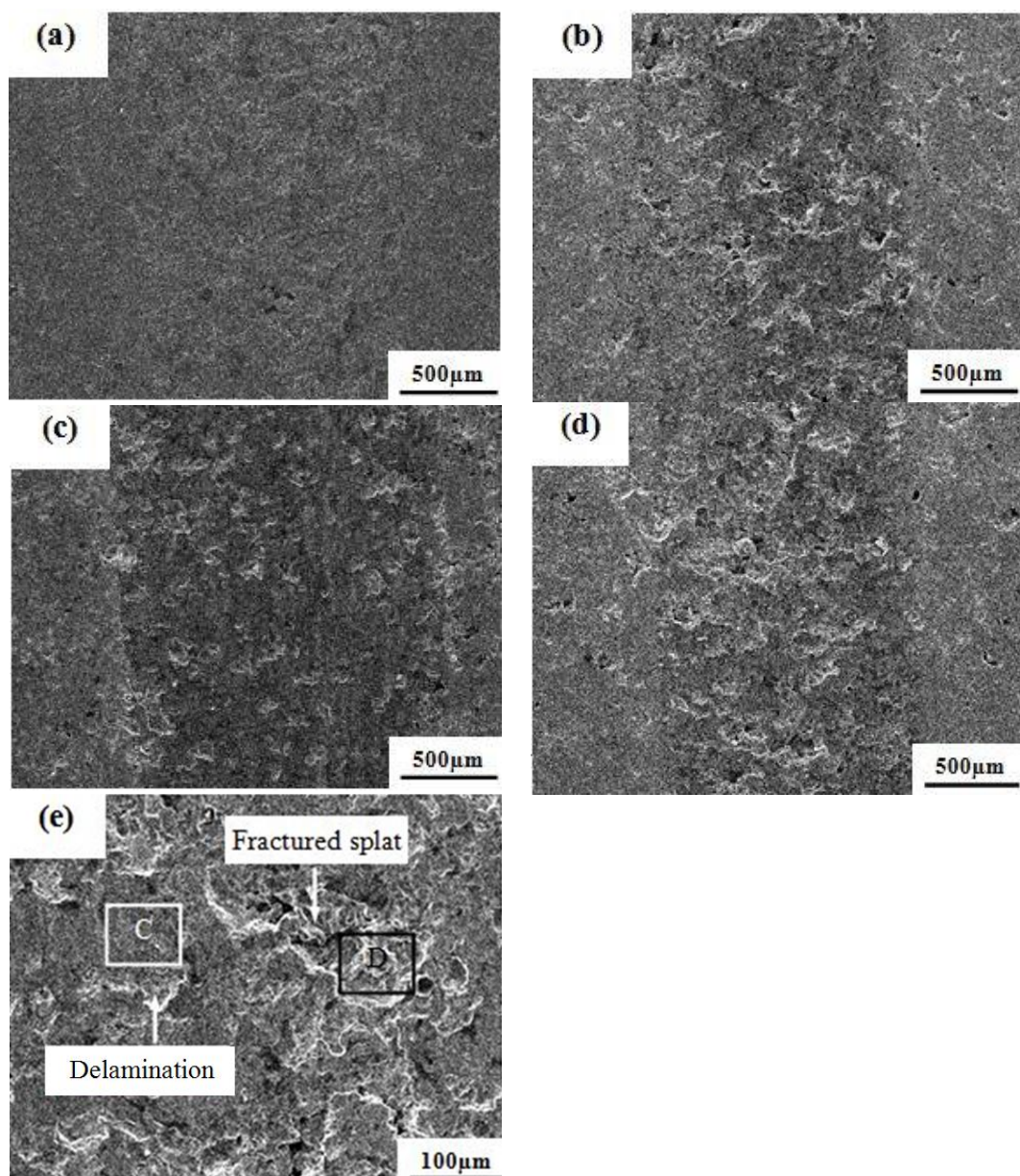


Figure 10. SEM morphologies of worn surface for Al_2O_3 -Mo coating at different temperatures: (a) RT; (b) 100 °C; (c) 200 °C; (d) 300 °C; (e) high-magnification morphology of (d).

To further illustrate the wear mechanisms of the coatings, wear tracks were investigated with EDS. The results are listed in Table 2. These results show that the worn surface of the Mo splats of two coatings contained Fe, Mo, and O elements, indicating that oxidation occurred during the wear process. The reciprocating motion caused the increase in temperature on the contact surface, which led to the oxidation. The presence of the Fe element indicates an adhesion wear between the coating and steel ball. Oxidation and adhesion wears are the main wear mechanisms of the two coatings. Based on the EDS analysis, the adhesion wear of the Mo coating was more severe compared to that of the Al₂O₃-Mo coating.

Table 2. Elemental composition of different zones in Figures 9e and 10e.

| Zone | Mo (at. %) | Fe (at. %) | O (at. %) |
|------|------------|------------|-----------|
| A | 99.2 | 0 | 0.8 |
| B | 65.2 | 13.9 | 20.9 |
| C | 91.2 | 3.2 | 5.6 |
| D | 99.4 | 0 | 0.6 |

In general, the friction and wear behaviors of a material depend on its microstructure, mechanical properties, and environmental conditions. During the wear test at RT, the metal oxide (MoO₃), which was formed in the APS process, played an important role in reducing the friction coefficient of the Mo coating. With an increase in the test temperature from RT to 300 °C, more severe decohesion and delamination of the splats appeared on the worn surface, causing the increase in surface roughness of the Mo coating. Meanwhile, the oxidation wear and adhesion wear increased, which resulted in a lot of adhesive metastases on the worn surface. Therefore, the friction coefficients increased with the further increases in test temperature. However, the worn surface of the Al₂O₃-Mo coating exhibited less signs of splats delamination, adhesion wear and lower roughness, causing the lower value of the friction coefficients, compared to those of the Mo coating.

The fracture and delamination of splats varied with the wear test temperature. This largely affected the wear rate of the coating. The fracture and delamination of splats became more and more severe (Figures 9 and 10), which resulted in an increase in the wear rates of the coatings. The hardness of a material also affects its wear properties. As mentioned above, strengthening with Al₂O₃ can provide the Mo coating with high hardness (Figure 5). The hardness of a steel counterpart is much higher than that of Mo coating. Thus, during dry sliding of the pure Mo coating, the steel counterpart will penetrate into the Mo coating. This results in a large removal of material due to plowing action. In the Al₂O₃-Mo coating, the contact interaction between the coating surface and the counterpart is mainly controlled by the strengthening Al₂O₃ particles. During the wear test, load-bearing Al₂O₃ particles protrude from the coating surface, which will reduce the direct contact area between the molybdenum part and steel ball and prevent a greater extent of wear.

4. Conclusions

In this work, the Mo and Al₂O₃-Mo coatings were fabricated by APS, using commercial Mo powders and mixed Al₂O₃-Mo powders respectively. The microstructure, mechanical properties, as well as the tribological properties from RT to 300 °C were comparably investigated. It is found that the porosity of the Mo coating (7.2 ± 0.4)% is much lower than that of the Al₂O₃-Mo coating (10.2 ± 0.5)%. The adhesion strength of Al₂O₃-Mo coating is about 33.6 ± 2.8 MPa, which is lower than the Mo coating adhesion strength of 43.8 ± 3.2 MPa. A hardness test showed that the addition of 30 wt. % Al₂O₃ increased the Mo coating hardness by 49.5%. The Al₂O₃-added Mo plasma-sprayed coating shows a lower friction coefficient and better wear resistance compared to the Mo coating. The main wear mechanisms of the two coatings were delamination, brittle fracture, oxidation and adhesion wear, and local plastic deformation, which were especially found in the Mo coating. However, in real application, due to numerous circumstantial factors, the situation could be more complicated.

Therefore, in further research, it is necessary to investigate the optimization of the amount of Al_2O_3 in order to maximize the mechanical properties under conditions that closely resemble real operation.

Author Contributions: J.Y. performed the experiments in addition to analyzing the data and writing the paper; Y.G. contributed the design of the experiments; Y.W. contributed the microstructure analysis of the samples; P.Z. have contributed with the revision of this paper; J.Q. conducted the analyzing of the experimental data.

Acknowledgments: This project was jointly supported by the National Natural Science Foundation of China (grant No. 51475161), the Scientific Research Fund of Hunan Provincial Education Department (Grant No. 15A059).

Conflicts of Interest: The authors declare no conflicts of interest.

References

1. Laribi, M.; Vannes, A.B.; Treheux, D. Study of Mechanical Behavior of Molybdenum Coating Using Sliding Wear and Impact Tests. *Wear* **2007**, *262*, 1330–1336. [[CrossRef](#)]
2. Farahmand, R.; Sohrabi, B.; Ghaffarinejad, A.; Meymian, M.R.Z. Synergistic effect of molybdenum coating and SDS surfactant on corrosion inhibition of mild steel in presence of 3.5% NaCl. *Corros. Sci.* **2018**, *136*, 393–401. [[CrossRef](#)]
3. Osadnik, M.; Wrona, A.; Lis, M.; Kamińska, M.; Bilewska, K.; Czepelak, M.; Czechowska, K.; Moskal, M.; Więclaw, G. Plasma-sprayed Mo-Re Coatings for Glass Industry Applications. *Surf. Coat. Technol.* **2017**, *318*, 349–354. [[CrossRef](#)]
4. Liu, Z.; Hua, M. Wear Transition and Mechanism in Lubricated Sliding of a Molybdenum Coating. *Tribol. Int.* **1999**, *32*, 499–506. [[CrossRef](#)]
5. Hwang, B.; Ahn, J.; Lee, S. Effects of Blending Elements on Wear Resistance of Plasma-Sprayed Molybdenum Blend Coatings Used for Automotive Synchronizer Rings. *Surf. Coat. Technol.* **2005**, *194*, 256–264. [[CrossRef](#)]
6. Wang, K.M.; Chang, B.H.; Chen, J.S.; Fu, H.G.; Lin, Y.H.; Lei, Y.P. Effect of Molybdenum on the Microstructures and Properties of Stainless Steel Coatings by Laser Cladding. *Appl. Sci.* **2017**, *7*, 1065. [[CrossRef](#)]
7. Modi, S.C.; Calla, E. A Study of High-Velocity Combustion Wire Molybdenum Coatings. *J. Therm. Spray Technol.* **2001**, *10*, 480–486. [[CrossRef](#)]
8. Sampath, S.; Wayne, S.F. Microstructure and Properties of Plasma-sprayed Mo-Mo₂C composites. *J. Therm. Spray Technol.* **1994**, *3*, 282–288. [[CrossRef](#)]
9. Yan, J.H.; He, Z.Y.; Wang, Y.; Qiu, J.W.; Wang, Y.M. Microstructure and Wear Resistance of Plasma-sprayed Molybdenum Coating Reinforced by MoSi₂ Particles. *J. Therm. Spray Technol.* **2016**, *26*, 1322–1329. [[CrossRef](#)]
10. Prchlik, L.; Gutleber, J.; Sampath, S. Deposition and Properties of High-Velocity-Oxygen-Fuel and Plasma-Sprayed Mo-Mo₂C Composite Coatings. *J. Therm. Spray Technol.* **2001**, *10*, 643–655. [[CrossRef](#)]
11. Debasish, D.; Mantry, S.; Behera, D.; Jha, B.B. Improvement of Microstructural and Mechanical Properties of Plasma Sprayed Mo Coatings Deposited on Al-Si Substrates by Premixing of Mo with TiN Powder. *High Temp.* **2014**, *52*, 19–25. [[CrossRef](#)]
12. Matikainen, V.; Niemi, K.; Koivuluoto, H.; Vuoristo, P. Abrasion, Erosion and Cavitation Erosion Wear Properties of Thermally Sprayed Alumina Based Coatings. *Coatings* **2014**, *4*, 18–36. [[CrossRef](#)]
13. Goel, S.; Björklund, S.; Curry, N. Axial Suspension Plasma Spraying of Al₂O₃ Coatings for Superior Tribological Properties. *Surf. Coat. Technol.* **2017**, *315*, 80–87. [[CrossRef](#)]
14. Deng, W.; Li, S.G.; Hou, G.L.; Liu, X.; Zhao, X.Q.; An, Y.L. Comparative study on wear behavior of plasma sprayed Al₂O₃ coatings sliding against different counterparts. *Ceram. Int.* **2017**, *43*, 6976–6986. [[CrossRef](#)]
15. Zhou, H.; Zhang, Y.P.; Hua, X.H.; Yang, Z.H.; Hou, S.Z.; Yu, Z.H. Al₂O₃/Mo Composite and Its Tribological Behavior Against AISI201Stainless Steel at Elevated Temperatures. *Int. J. Refract. Met. Hard Mater.* **2014**, *43*, 263–268. [[CrossRef](#)]
16. Ghasemi, R.; Vakilifard, H. Plasma-sprayed nanostructured YSZ thermal barrier coatings: Thermal insulation capability and adhesion strength. *Ceram. Int.* **2017**, *43*, 8556–8563. [[CrossRef](#)]
17. Davis, J.R. *Hand Book of Thermal Spray Technology*, 1st ed.; ASM International: Materials Park, OH, USA, 2004.
18. Yan, J.H.; Wang, Y.; Liu, L.F.; Wang, Y.M.; Chen, F. Preparation of Protective MoSi₂ Coating on Niobium Substrate. *J. Therm. Spray Technol.* **2015**, *24*, 1093–1099. [[CrossRef](#)]
19. Planche, M.P.; Liao, H.; Coddet, C. Oxidation Control in Atmospheric Plasma Spraying Coating. *Surf. Coat. Technol.* **2007**, *202*, 69–76. [[CrossRef](#)]

20. Gao, P.H.; Yang, G.J.; Cao, S.T.; Li, J.P.; Yang, Z.; Guo, Y.C. Heredity and Variation of Hollow Structure from Powders to Coatings Through Atmospheric Plasma Spraying. *Surf. Coat. Technol.* **2016**, *305*, 76–82. [[CrossRef](#)]
21. Wan, D.T.; Zhou, Y.C.; Bao, Y.W. Evaluation of the elastic modulus and strength of unsymmetrical Al₂O₃ coating on Ti₃SiC₂ substrate by a modified relative methodology. *Mater. Sci. Eng. A* **2008**, *474*, 64–70. [[CrossRef](#)]
22. Cockeram, B.V. The mechanical properties and fracture mechanisms of wrought low carbon arc cast (LCAC), molybdenum-0.5pct titanium-0.1pct zirconium (TZM), and oxide dispersion strengthened (ODS) molybdenum flat products. *Mater. Sci. Eng. A* **2006**, *418*, 120–136. [[CrossRef](#)]
23. Fei, X.; Niu, Y.; Ji, H.; Zheng, X.B. A Comparative Study of MoSi₂ Coatings Manufactured by Atmospheric and Vacuum Plasma Spray Processes. *Ceram. Int.* **2011**, *37*, 813–817. [[CrossRef](#)]
24. Yan, J.H.; Zhang, Z.; Liu, L.F.; Xu, H.M.; Mao, Z.Y. Effect of Nano-ZrO₂ on the Microstructure and High Temperature Tribological Properties of MoSi₂ Coating. *J. Therm. Spray Technol.* **2013**, *22*, 873–881. [[CrossRef](#)]
25. Zha, X.M.; Jiang, F.; Xu, X.P. Investigating the high frequency fatigue failure mechanisms of mono and multilayer PVD coatings by the cyclic impact tests. *Surf. Coat. Technol.* **2018**, *344*, 689–701. [[CrossRef](#)]
26. Hwang, B.; Lee, S.; Ahn, J. Correlation of Microstructure and Wear Resistance of Molybdenum Blends Coatings Fabricated by Atmospheric Plasma Spraying. *Mater. Sci. Eng. A* **2004**, *366*, 152–163. [[CrossRef](#)]



© 2018 by the authors. Licensee MDPI, Basel, Switzerland. This article is an open access article distributed under the terms and conditions of the Creative Commons Attribution (CC BY) license (<http://creativecommons.org/licenses/by/4.0/>).